^{57}Fe Mössbauer study of $NiFe_2O_4$ nanoparticles produced by the levitation-jet aerosol technique

Lara K. Bogart[1] · Iurii G. Morozov[2] · Ivan P. Parkin[3] · Maksim V. Kuznetcov[*4]

Abstract For the first time, Mössbauer parameters of mixed cubic spinel $NiFe_2O_4$ nanoparticles, prepared by using a one-stage process *via* evaporation of levitating iron-nickel droplets into a mix of helium-air gas flow accompanied with the application of a DC electric field of up to 210 kVm^{-1}, are reported.

Keywords:

^{57}Fe Mössbauer spectroscopy

Nickel ferrite

Nanoparticles

Levitation-jet technique

Applied electric field

XRD

1 Introduction

Nickel ferrite ($NiFe_2O_4$) is an intensively studied soft magnetic material due to their excellent properties as large saturation magnetization, excellent chemical stability and corrosion resistance, which results in its highly complex permeability over a wide frequency range [1], as well as good electromagnetic performance and chemical stability [2]. For this reason, it can be used in various applications, such as magnetic resonance imaging, microwave devices, transformer cores, or sensors etc. [3]. Nickel ferrite nanoparticles (NPs) has attracted a considerable attention because of their technological importance in industrially developed areas such as microwave devices in the GHz region, high-speed magnetic media recording, magnetic refrigeration systems as well as catalysts [4-7]. For example, such NPs can be readily applied on the reduced graphene oxides nanosheets as a multi-functional microwave absorption material in various fields ranging from civil engineering and commerce to the military and aerospace industry [8, 9].

✉ Maksim V. Kuznetcov
maxim1968@mail.ru

1 Healthcare Biomagnetics Laboratory, University College London, 21 Albemarle Street, London W1S 4BS, UK
2 Merzhanov Institute of Structural Macrokinetics and Materials Science, Russian Academy of Sciences, Chernogolovka, Moscow Region, 142432, Russia
3 Department of Chemistry, Materials Chemistry Research Centre, University College London, London WC1H 0AJ, UK
4 All-Russian Research Institute on Problems of Civil Defense and Emergencies of Emergency Control Ministry of Russia (EMERCOM), 121352, Russia

NPs usage in all the above-mentioned applications is critically dependent on the combination of their unique physical, chemical, and magnetic properties, which, in turn, are intrinsically related to the distribution of divalent and trivalent cations amongst interstitial sites. But, ^{57}Fe Mössbauer spectra as one of the main technique for determination of such distribution in the nickel ferrites NPs, has been relatively poor reported previously in the literature [10, 11]. Particularly, nanosized $NiFe_2O_4$ powders prepared by a wet sol-gel route *via* calcination at 1200°C and subsequently quenched by liquid nitrogen, has an average crystallite size of 67 nm and also exhibited a mixed spinel phase with a saturation magnetization of about 49 Am^2kg^{-1}, which is close to that of bulk $NiFe_2O_4$. The Mössbauer parameters for that materials are follows: hyperfine magnetic field B_1 = 52 T, B_2 = 48.4 T, and A = 48.8 T [10]. The Mössbauer spectrum of NPs, prepared using a natural proteic solution of coconut water with metal ions and subsequently annealed at 400°C (with an average crystallite size of 5 nm) is representing as a superparamagnetic doublet, whilst all the samples, which has been treated at above 800°C, has crystallite sizes larger ≥ 30 nm with a magnetic sextet structure reminiscent of a mixed spinel phase [11]. In this work, we have determined for the first time Mössbauer parameters of mixed spinel $NiFe_2O_4$ NPs, prepared using a dry gas-phase aerosol levitation-jet synthesis accompanied with the application of a DC electric field, which was used to adjust the NPs average particle size and phase composition.

2 Experimental section

The studied aerosol-generated $NiFe_2O_4$ NPs were synthesized by using a one-stage dry levitation-jet process in presence of an applied DC electric field, which was described in detail elsewhere [12-14]. In this technique a piece of metallic nickel wire (1 g) was wound around an iron wire in a volume ratio of Ni:Fe = 1:2 and suspended in a quartz tube with an inner diameter of 14 mm. This seed was subsequently heated *via* the application of electromagnetic field (0.44 MHz) of a counter-current inductor until fusion into an iron-nickel droplet which first levitated in the tube and then started its evaporation. The evaporated droplet was blown by descending helium gas flow, resulting in its condensation at which point it was continuously fed with nickel and iron wires at a pre-set rate using a purpose-designed device in the volume ratio indicated above. The source wired materials were a 0.2 mm in diameter for the NP-1 pure nickel wire and a 0.3 mm in diameter for the Prov1 low-carbon iron wire (RF State Standard GOST 3282-74). Nickel ferrite nanoparticles were finally obtained by adding a small amount of air the flowing gas upstream of the droplet; the amount of air was determined by the concurrence of the highest flow rate with a stability of the synthesis process for the preparation of NPs with controlled average sizes. During

the synthesis process, an electric field was applied to the condensation/cooling zone near the levitating droplet as well as in a transverse direction to the gas flow by means of two thin tungsten rods, anchored outside the quartz tube, which generated a DC electric field between 0 and 210 kV/m. Such geometry allows the electric field to act over a cooling zone and provides crystallization of metal vapor into nanoparticles [12].

Since the applied electric field may affect both crystallization and oxidation processes [15, 16], it results in the limitation on the mutual diffusion of nickel, iron, and oxygen atoms and the occurrence of the numerous dynamic processes involved in the solid state reactions, including both metals atoms nucleation and surface oxygen diffusion could take place [17]. This phenomenon may take place because of oxygen ionization processes in the vapor condensation zone. The formation and evolution of mixed oxide domains in the particles are also primarily dictated by the surface oxygen dynamics - uptake and surface mobility, which are strongly depended on the applied electric field. At zero electric field, the activation energy barriers for ionic migration are still high enough to ensure lower oxygen surface mobility [16]. Increasing the oxygen partial pressure increases the rate of oxide nucleation, which couples to the enhanced surface mobility of oxygen atoms in the presence of electric field [12].

So, the above-described process yielded mixed cubic spinel ferrite NPs – so-called the 'M-series' - with average sizes ranging from 30 up to 70 nm (Table 1).

NPs morphology and particle sizes were examined using scanning electron microscope (SEM) CARL ZEISS ULTRA PLUS, operated at 15 kV, and transmission electron microscopy (TEM) using a JEOL JEM100CX II, operated at 100 kV. Electron micrographs were analyzed using Carl Zeiss AxioVision SE64 ver. 4.91 image processing software and size distribution of the particles and their volume average size *D* were determined. Crystal structures of NPs were determined by X-ray powder diffractometer DRON-3M (Cu K_α radiation). Their phase compositions were determined using JCPDS PDF (release 2011) and Crystallographica SearchMatch v. 3.102 software. Rietveld analysis (PowderCell 2.0 software) of X-ray diffraction patterns was applied to evaluate the fraction of crystalline phases in nanoparticles. ^{57}Fe Mössbauer spectroscopy was performed at room temperature using a SeeCo Inc., (USA) spectrometer. Spectra were recorded using a ^{57}Co in Rh foil as the source of 14.4 keV γ-rays, which were driven at constant acceleration mode and recorded in a SeeCo Inc., W302 detector.

Table 1 Comparison of selected synthesis conditions and chemical compositions ascertained from Mössbauer spectra for samples prepared under similar conditions, but under the different electric fields applied to the reaction zone during synthesis processes

Sample	Selected structural parameters			Mössbauer fitting parameters				
	D (nm)	*a* (nm)	*E* (kVm^{-1})	$NiFe_2O_4$ (%)	Unreacted Fe (%)	Fe_xNi_{1-x} (%)	$\langle H_{hf} \rangle$ (T)	Fe_xNi_{1-x} suggested stoichiometry
M13	36	0.83384	0	75.0	1.6	23.4	29.1	$Fe_{20}Ni_{80}$
M14	31	0.83408	210	81.5	0.9	17.6	28.5	$Fe_{25}Ni_{75}$
M15	69	0.83400	105	14.0	5.1	80.9	23.3	$Fe_{65}Ni_{35}$
M19	53	0.83396	165	40.0	4.9	55.1	22.7	$Fe_{65}Ni_{35}$

3 Results and discussion

X-ray analysis confirms that all the samples prepared using this synthesis process were fully crystallized compounds, with cubic spinel $NiFe_2O_4$ (Fd3m) unit cell parameters, which were in the full agreement with reference data JCPDS 74-2081, 10-0325, and 44-1485 (a = 0.83384 - 0.83408 nm) [13, 18-20]. Fig. 1 compares the XRD patterns of NPs prepared under similar conditions, but with the different electric fields applied to the reaction zone during the synthesis process. An electric field of up to 210 kVm^{-1} application has a strong effect on the phase composition of the NPs, leading to the presence of unreacted iron as well as partially oxidized Fe-Ni alloy. In contrast to those results, the application of an electric field strength of 210 kV/m resulted in almost single-phase NPs.

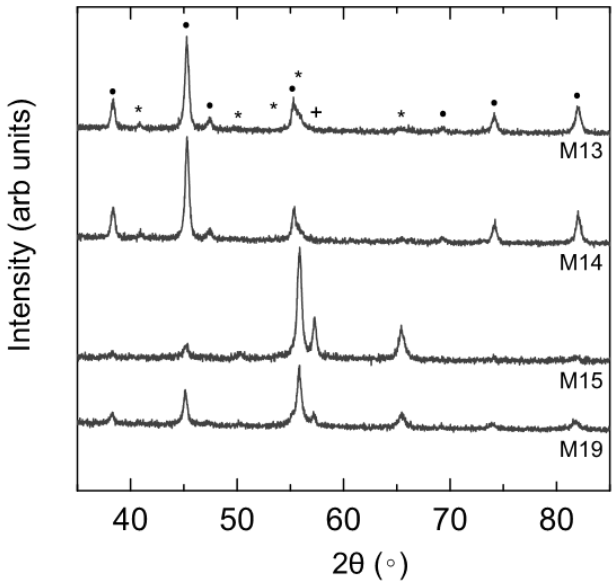

Fig. 1 XRD patterns of NPs prepared using aerosol assisted levitation-jet and with an application of various electric fields: M13 – 0 kVm^{-1}, M15 – 105 kVm^{-1}, M19 – 165 kVm^{-1} and M14 – 210 kVm^{-1}. Miller indices correspond to $NiFe_2O_4$ (•); FeNi (*) and unreacted Fe (+) respectively

Morphological, structural and DC magnetic parameters of the samples under study were partially examined previously [13]. As it is seen, for example, from the Fig. 2, the main quantity of sample M14 particles has a pseudospherical 14-hedron shape with a small scatter in particle size, which follows a log-normal distribution [13]. A comparative morphological analysis of particles projections in all the micrographs allows evaluating the average nanoparticle size (*D*), which is presented in Table 1. It was established, that NPs synthesized under zero electric field tend to have a much broader size distribution than those prepared under non-zero field [13]. In the case of M14 NPs, particles are present in the form of hexagonal platelets with a regular aspect ratio—whereas for NPs M15 and M19 NPs, core-shell structures with a shape between spherical and hexagonal types are evident from the corresponding images [13]. So, the DC electric field application may aid in controlling the oxidation reactions [21, 22], also providing the additional control of size, morphology and phase composition of NPs.

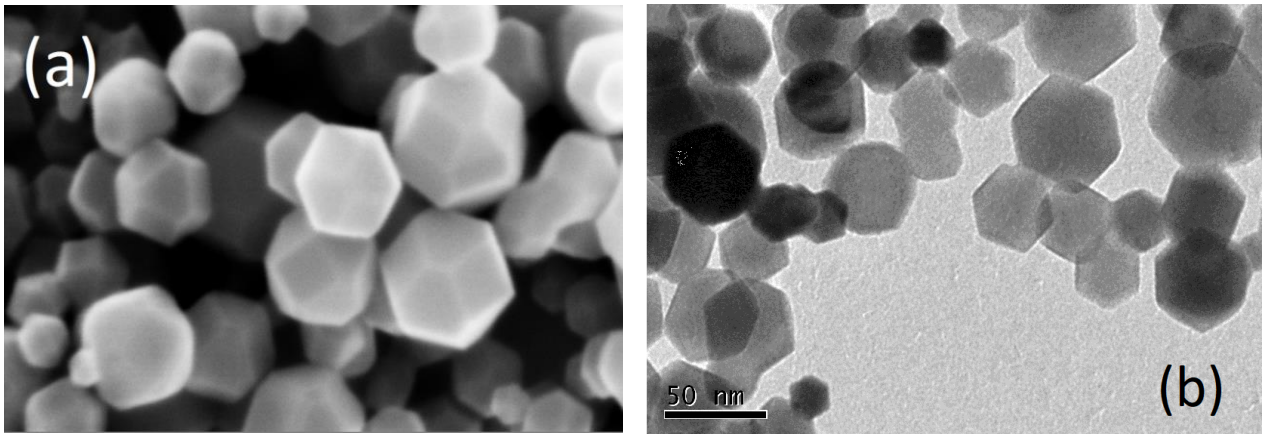

Fig. 2 SEM (a) and TEM (b) images of NPs M14. Figures (a) and (b) have the same scale bar values

Table 1 providing few correlations between the selected synthesis conditions and chemical compositions obtained from Mössbauer spectra. It should be noted that all the spectra were folded and baseline corrected relative to the 10 μm thick α-Fe foil at room-temperature (RT) and subsequently fitted using Voigtian shaped line profiles in Recoil [23-25]. Voigtian linewidths have been used to represent Gaussian distributions of Lorentzian lines, and so reflect a distribution of hyperfine fields. This may have physical origins from either range of crystallographic quality, surface spins, number of crystallite sizes or combination of all three.

Visual inspection of the spectra in Figure 3 shows that α-Fe exists in all samples as indicated by the paramagnetic doublet at the center of each spectrum. Interestingly, XRD measurements indicate the presence of Fe in samples of M15 and M19 only. All spectra were fitted using a model that assumed the presence of Fe in three phases: ferrimagnetic $NiFe_2O_4$ (i.e. two sextets arising from Fe^{3+} on both tetrahedral and octahedral sites), ferromagnetic Fe_xNi_{1-x} (one sextet of Fe^0) and paramagnetic α-Fe (singlet, Fe^0). For all samples, starting values of bulk $NiFe_2O_4$ and $Fe_{33}Ni_{67}$ were used to apply the initial model of the observed spectra [13, 26], after which all the fitting parameters were subsequently allowed to float with the only constraint being the maintenance of the area of absorption lines ratio 3:2:1 [24]. RT spectra and best-fit spectra (lowest χ^2) are shown in Fig. 3 with details of fitting parameters provided in Table 2.

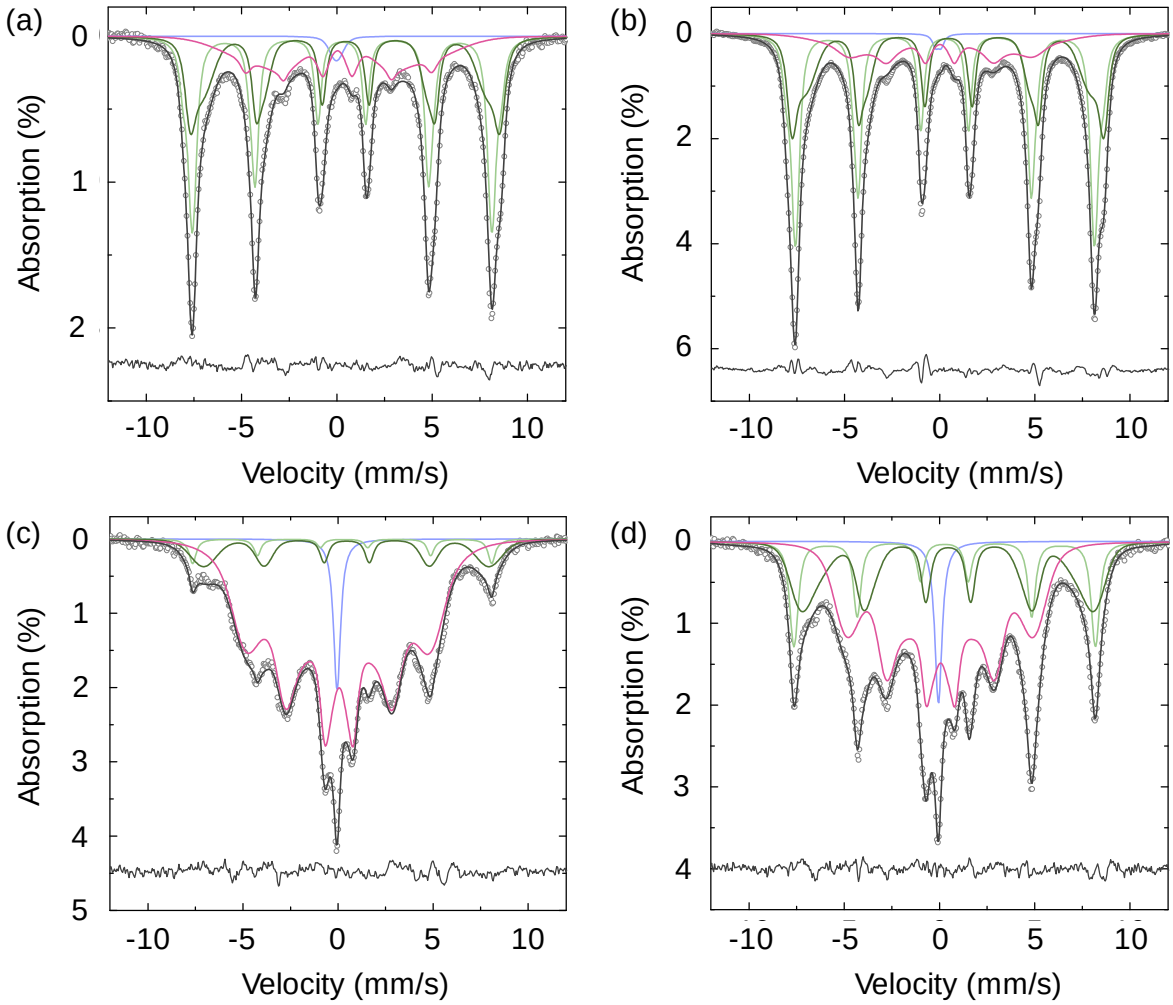

Fig. 3 Room temperature ^{57}Fe Mössbauer spectra of (a) M13, (b) M14, (c) M15 and (d) M19 nanoparticles. The solid grey lines represent the best-fit results of the recorded spectra (*open circles*), with the quality of fit indicated by residual. Sub-components are indicated as follows: green Fe^{3+} (*light green A site, dark green B site*); paramagnetic α-Fe (*blue*); Fe^0 in the form Fe_xNi_{1-x} (*pink*)

Table 2 Best-fit parameters to the Mössbauer spectra showing isomer shift (δ), quadrupole splitting (*Q*), hyperfine field (H_{hf}) and relative spectral area *S* for each Fe phase

Sample	δ (mm/s)	*Q* (mm/s)	ε (mm/s)	H_{hf} (T)	w3 (mm/s)	*S* (%)	Phase
M13	-0.0220	0, σ =0.51	-	-	0.21	1.6	Fe^0
	0.2676	-	0.0065	51.7 σ = 4.4		16.0 40.5 84.0	Fe^{3+} (*A site*)
				48.7 σ = 6.3			
	0.4468		-0.0124	46.4 σ = 30.6		62.0 34.6 38.0	Fe^{3+} (*B site*)
				50.4 σ = 9.1			
	0.0644		0.0335	289 σ = 98.8		88.2 23.3 11.8	Fe-Ni
				30.3 σ = 9.1			
M14	-0.0759	0.29, σ = 0.04	-		0.19	0.90	Fe^0
	0.2676		0.0065	51.7 σ = 4.4		16.0 44.3 84.0	Fe^{3+} (*A site*)
				48.7 σ = 6.3			
	0.4468		-0.0124	46.5 σ = 30.6		58.6 37.2 41.4	Fe^{3+} (*B site*)
				50.9 σ = 8.3			
	0.0305		0.0220	28.1 σ = 109		77.8 17.6 22.2	Fe-Ni
				30.0 σ = 28.8			
M15	-0.050	0, σ =0.07	-		0.21	5.1	Fe^0
	0.2676	-	-0.502	51.6 σ = 2.1		3.9 3.4 96.1	Fe^{3+} (*A site*)
				48.8 σ = 1.4			
	0.4468		-0.0123	46.5 σ = 35		74.1 10.6 25.9	Fe^{3+} (*B site*)
				47.1 σ = 50			
	0.0322		-0.0268	30.3 σ = 35.6		29.1 80.9 70.9	Fe-Ni
				20.5 σ = 118.5			
M19	0.0539	0, σ =0.04	-	-	0.23	4.9	Fe^0
	0.2676	-	0.0065	66.3 σ = 53		3.4 14.8 96.6	Fe^{3+} (*A site*)
				49.1 σ = 5.6			
	0.4468		-0.0123	43.2 σ = 42.2		46.0 25.2 54.0	Fe^{3+} (*B site*)
				48.2 σ = 28.0			
	0.0499		-0.0097	17.7 σ = 105		60.9 55.1 39.1	Fe-Ni
				30.6 σ = 633			

All the spectra have broad absorption peaks, which is indicative of fine particle nature of the samples. For M13 and M14 samples, the majority of absorption arises from Fe^{3+}, located on A and

B sites of the $NiFe_2O_4$ spinel, which comprises more than 75% (82%) of the sample, respectively. These two components have isomer shifts, (δ) at approximately 0.27 mm/s and 0.45 mm/s, with mean hyperfine fields close to 49 T and 48 T, respectively. The values of hyperfine fields observed here are smaller than that of the bulk – 50.6 T and 54.8 T, respectively, which may be attributed to the presence of collective excitations, arises from the nanoscale dimensions of particles. The third sextet comprises ca. 23% (18%) of the spectral area, with δ close to zero, indicating the presence of Fe^0, and a mean hyperfine field of ca. 29.0 T and 28.5 T, respectively. Interestingly, we observed that the large electric field (210 kVm^{-1}) application during synthesis has a very little effect on the hyperfine field values at the ^{57}Fe nucleus, in contrast to the magnetic properties of our NPs discussed in Ref. [13]. This field is related to the stoichiometry of Fe-Ni alloys and, using Johnson *et al.*, we surmise that the composition corresponds to a nickel content of *ca*. 85% (75%), respectively [27].

Finally, the best-fit model includes singlet at the center of the spectrum, which indicates a small amount of paramagnetic α-Fe (1.6% and 0.9%, respectively) within both samples. Interestingly, this Key Mössbauer fitting parameters and deduced chemical compositions are sequentially compared to the synthesis conditions in Table 1.

The Mössbauer spectra of M15 and M19 samples clearly indicate that the predominant phase is the Fe-Ni alloys with less than 50% of the material with respect to the intended $NiFe_2O_4$ phase. In M15 NPs we observed, that ca. 81% of absorption arises from Fe^0 in FeNi, although this is slightly less, then in M19 at ca. 55%. In both samples, the mean hyperfine field of this phase is, approximately, 23 T and indicates a nickel content of close to 35 *at*.%. For M15 NPs, the best-fit model indicates, that the remaining content is 14% (40%) of $NiFe_2O_4$ and 5% of α-Fe, which are in a good agreement with XRD data (Figure 1).

4 Conclusions

In conclusion, small changes in the synthesis conditions of $NiFe_2O_4$ nanoparticles prepared using the levitation-jet aerosol process has made a significant effect on both the crystallite size and chemical composition of the nanoparticles. The DC electric field has a strong effect on the phase composition of the samples, leading to the presence of unreacted Fe and partially oxidized Fe_xNi_{1-x} alloy. It is only with ^{57}Fe Mössbauer spectroscopy that we can precisely identify and indeed quantify, of all Fe-based phases present. Our analysis has revealed the presence of unreacted Fe close to 1% in spectral area, and which was unresolvable by X-ray diffraction, as well as allowing for the quantification of the of Fe_xNi_{1-x} phases stoichiometry. The electric field reduces the nucleation and growth rates, eventually reducing the size of resulting nanoparticles and changing

their phase compositions. Levitation-jet synthesis in the presence of large electric fields (up to 210 kVm^{-1}) produces small crystallites of 31 nm, that are predominately $NiFe_2O_4$ as the predominant phase (> 75%) with ca. 18% $Fe_{25}Ni_{85}$ with the remainder (<1%), is unreacted α-Fe. For intermediate electric fields (105 kVm^{-1}), ca. 80% of the sample is $Fe_{65}Ni_{35}$ and only 14% is the desired $NiFe_2O_4$. Thus, ^{57}Fe Mössbauer spectroscopy usage is an invaluable tool for the optimization of synthesis methods of high-quality nickel ferrite nanoparticles.

References

[1] X. Gu, W. Zhu, C. Jia, R. Zhao, W. Schmidt, Y. Wang, Synthesis and microwave absorbing properties of highly ordered mesoporous crystalline $NiFe_2O_4$, Chemical Communications 47(18) (2011) 5337-5339.
[2] P. Hernández-Gómez, J.M. Muñoz, M.P.F. Graça, M.A. Valente, Magnetic after-effects in Ni ferrite nanoparticles, Materials Letters 225 (2018) 62-64.
[3] T. Ahmad, H. Bae, Y. Iqbal, I. Rhee, S. Hong, Y. Chang, J. Lee, D. Sohn, Chitosan-coated nickel-ferrite nanoparticles as contrast agents in magnetic resonance imaging, Journal of Magnetism and Magnetic Materials 381 (2015) 151-157.
[4] Z.H. Zhou, J.M. Xue, J. Wang, H.S.O. Chan, T. Yu, Z.X. Shen, $NiFe_2O_4$ nanoparticles formed in situ in silica matrix by mechanical activation, Journal of Applied Physics 91(9) (2002) 6015-6020.
[5] R.H. Kodama, Magnetic nanoparticles, Journal of Magnetism and Magnetic Materials 200(1) (1999) 359-372.
[6] S. Prasad, N.S. Gajbhiye, Magnetic studies of nanosized nickel ferrite particles synthesized by the citrate precursor technique, Journal of Alloys and Compounds 265(1) (1998) 87-92.
[7] M.P. Pileni, Magnetic Fluids: Fabrication, Magnetic Properties, and Organization of Nanocrystals, Advanced Functional Materials 11(5) (2001) 323-336.
[8] J.-Z. He, X.-X. Wang, Y.-L. Zhang, M.-S. Cao, Small magnetic nanoparticles decorating reduced graphene oxides to tune the electromagnetic attenuation capacity, Journal of Materials Chemistry C 4(29) (2016) 7130-7140.
[9] Y. Zhang, X. Wang, M. Cao, Confinedly implanted $NiFe_2O_4$-rGO: Cluster tailoring and highly tunable electromagnetic properties for selective-frequency microwave absorption, Nano Research 11(3) (2018) 1426-1436.
[10] M.N.B. Silva, J.G.d.S. Duque, D.X. Gouveia, J.A.C. de Paiva, M.A. Macedo, Novel Route for the Preparation of Nanosized $NiFe_2O_4$ Powders, Japanese Journal of Applied Physics 43(8R) (2004) 5249.
[11] J.A.C. de Paiva, M.P.F. Graça, J. Monteiro, M.A. Macedo, M.A. Valente, Spectroscopy studies of $NiFe_2O_4$ nanosized powders obtained using coconut water, Journal of Alloys and Compounds 485(1) (2009) 637-641.
[12] Y.G. Morozov, O.V. Belousova, M.V. Kuznetsov, D. Ortega, I.P. Parkin, Electric field-assisted levitation-jet aerosol synthesis of Ni/NiO nanoparticles, Journal of Materials Chemistry 22(22) (2012) 11214-11223.
[13] D. Ortega, M.V. Kuznetsov, Y.G. Morozov, O.V. Belousova, I.P. Parkin, Thermal relaxation and collective dynamics of interacting aerosol-generated hexagonal $NiFe_2O_4$ nanoparticles, Physical Chemistry Chemical Physics 15(48) (2013) 20830-20838.

[14] I.G. Morozov, S. Sathasivam, O.V. Belousova, I.V. Shishkovsky, M.V. Kuznetcov, Room temperature ferromagnetism in mixed-phase titania nanoparticles produced by the levitation–jet generator, Journal of Materials Science: Materials in Electronics 29(4) (2018) 3304-3316.
[15] D.A. Ksenofontov, L.N. Dem'yanets, A.K. Ivanov-Schitz, Electric-field effect on crystal growth in the Li_3PO_4-Li_4GeO_4-Li_2MoO_4-LiF system, Inorg. Mater. 44(10) (2008) 1115-1120.
[16] S.K.R.S. Sankaranarayanan, S. Ramanathan, Electric Field Control of Surface Oxygen Dynamics and its Effect on the Atomic Scale Structure and Morphology of a Growing Ultrathin Oxide Film, J. Phys. Chem. C. 114(14) (2010) 6631–6639.
[17] M.A. Albao, F.-C. Chuang, J.W. Evans, Kinetic Monte Carlo simulation of an atomistic model for oxide island formation and step pinning during etching by oxygen of vicinal Si(100) Thin Solid Films 517 (2009) 1949-1957.
[18] K. Maaz, S. Karim, A. Mumtaz, S.K. Hasanain, J. Liu, J.L. Duan, Synthesis and magnetic characterization of nickel ferrite nanoparticles prepared by co-precipitation route, Journal of Magnetism and Magnetic Materials 321(12) (2009) 1838-1842.
[19] M. Srivastava, S. Chaubey, A.K. Ojha, Investigation on size dependent structural and magnetic behavior of nickel ferrite nanoparticles prepared by sol–gel and hydrothermal methods, Materials Chemistry and Physics 118(1) (2009) 174-180.
[20] M.G. Naseri, E.B. Saion, H.A. Ahangar, M. Hashim, A.H. Shaari, Simple preparation and characterization of nickel ferrite nanocrystals by a thermal treatment method, Powder Technology 212(1) (2011) 80-88.
[21] M.V. Kuznetsov, S.M. Busurin, Y.G. Morozov, I.P. Parkin, Heterogeneous combustion in electrical and magnetic fields: modification of combustion parameters and products, Phys. Chem. Chem. Phys. 5 (2003) 2291-2296.
[22] Y.G. Morozov, O.V. Belousova, M.V. Kuznetsov, Preparation of Nickel Nanoparticles for Catalytic Applications, Inorg. Mater. 47(1) (2011) 36-40.
[23] J. Fock, L.K. Bogart, O. Posth, M.F. Hansen, Q.A. Pankhurst, C. Frandsen, Uncertainty budget for determinations of mean isomer shift from Mössbauer spectra, Hyperfine Interactions 237(1) (2016) 23.
[24] J. Fock, L.K. Bogart, D.G. Alonso, J.I. Espeso, M.F. Hansen, M. Varon, C. Frandsen, Q.A. Pankhurst, Unpublished Manuscript 2017.
[25] K. Lagarec, D.G. Rancourt, Recoil-Mössbauer spectral analysis software for Windows, University of Ottawa, Ottawa, ON (1998).
[26] C.N. Chinnasamy, A. Narayanasamy, N. Ponpandian, K. Chattopadhyay, K. Shinoda, B. Jeyadevan, K. Tohji, K. Nakatsuka, T. Furubayashi, I. Nakatani, Mixed spinel structure in nanocrystalline $NiFe_2O_4$, Physical Review B 63(18) (2001) 184108.
[27] C.E. Johnson, M.S. Ridout, T.E. Cranshaw, The Mössbauer Effect in Iron Alloys, Proceedings of the Physical Society 81(6) (1963) 1079.